A new definition of the kinematic breaking onset criterion validated with solitary and quasi-regular waves in shallow water

Audrey Varing*[a], Jean-Francois Filipot[a], Stephan Grilli[b], Rui Duarte[a], Volker Roeber[c], Marissa Yates[d,e]

[a] *France Energies Marines, Bâtiment Cap Océan, 525 avenue Alexis de Rochon, 29280 Plouzané - France*
[b] *Department of Ocean Engineering, University of Rhode Island, Narragansett, RI, USA*
[c] *Université de Pau et des Pays de l'Adour, Allée du Parc Montaury, 64600 Anglet, France*
[d] *Saint-Venant Hydraulics Laboratory, Université Paris-Est (joint research unit EDF R&D, Cerema, ENPC), 6 quai Watier, BP 49, 78401 Chatou, France*
[e] *Cerema, Technical Department of Water, Sea and Rivers, 29280 Plouzané, France*

Abstract

A large body of work has been devoted to the accurate detection and simulation of wave breaking in coastal areas. It is a key process for a wide range of engineering activities and environmental issues. This has motivated the development of a variety of breaking onset criteria, such as kinematic criteria based on a maximum value (usually unity) of the ratio u_c/c, of the horizontal particle velocity at the wave crest u_c to its phase velocity c, both taken in the direction of wave propagation. Here, we numerically investigate the validity of this criterion in capturing breaking onset for solitary and quasi-regular two-dimensional shallow water waves using the Fully Nonlinear Potential Flow (FNPF) model by Grilli and Subramanya (1996). With this model, the propagation up to overturning of solitary waves over plane slopes, and solitary and quasi-regular waves over a submerged bar, both initially specified as numerically exact FNPF waves, is simulated. In all cases, waves break as spilling or plunging breakers, initiated by the formation of a breaker jet near the wave crest. Results show that the location of the maximum fluid velocity $\|\mathbf{u}\|_m$ on the free surface closely coincides with the location where the overturning jet is initiated. Based on this, a new breaking onset criterion is proposed as $\|\mathbf{u}\|_m/c \simeq 1$, which is shown to be more universal for accurately detecting wave breaking initiation than existing criteria based on the crest velocity.

Keywords: Wave breaking onset, depth-induced breaking, kinematic wave breaking criterion, nearshore waves, Fully Nonlinear Potential Flow model.

1. Introduction

Wave breaking is a key nearshore process for a wide range of engineering activities and environmental issues. Breaking waves cause the largest hydrodynamic loads on marine and coastal structures. In addition, energy dissipation resulting from wave breaking is also the primary control of the wave height cross-shore evolution, the wave setup magnitude, and the generation of infragravity waves and wave-induced currents that drive sediment erosion and transport [1, 2, 3, 4, 5, 6]. Accordingly, a significant amount of work has been devoted to the accurate simulation or parameterization of wave breaking in nearshore numerical wave propagation models. Wave models not based directly on the primitive Navier-Stokes equations [e.g. 7, 8, 9], require wave breaking to be parameterized. Breaking must first be detected using an appropriate breaking onset criterion, and then an appropriate amount of energy dissipation must be specified over the grid area deemed to be breaking. The latter has been achieved based on different methods such as empirical eddy

*Corresponding author. E-mail address : audrey.varing@ite-fem.org

viscosity, sponge layer or shock capturing algorithm [e.g. 10, 11]. Over the past half century, many breaking onset criteria have been proposed for a variety of practical applications based on theoretical studies, numerical simulations, laboratory experiments, or field observations [e.g. 12, 13]. Such criteria are typically classified into three categories: geometric, kinematic, and dynamic.

1.1. Geometric breaking criteria

By studying regular waves propagating over a flat bottom, [14] showed that wave breaking is initiated when $kH/\tanh(kh) = 0.88$, with $k = 2\pi/\lambda$ the wavenumber, H the wave height, λ the wavelength, and h the water depth. In shallow water, Miche's criterion transforms into the breaker index criterion, $\gamma = H/h = \gamma_m$, where γ_m is a function of the beach slope and the incident wave steepness. Widely used in the literature [e.g. 15, 16], this approach has proven to be adequate for initiating wave breaking dissipation in phase-averaged spectral models [e.g. 17]. In phase-resolving wave models, a maximum slope criterion for the wave front face has also been used to detect the onset of breaking [e.g. 18, 9, 19, 20], but the maximum slope value used varies widely between different studies [e.g. 21, 22, 23, 24, 19], which poses the question of the generality and applicability of such breaking onset criteria.

1.2. Kinematic breaking criteria

Kinematic breaking criteria are typically based on a threshold value of the ratio between the horizontal fluid velocity at the wave crest (defined as the maximum free surface elevation) u_c, and the local wave phase speed c, both taken in the direction of wave propagation [e.g. 25, 26]. Wave breaking is assumed to occur when u_c exceeds c, i.e. $u/c \geq 1$, corresponding to crest overturning and the local formation of a breaker jet (see e.g. [27] for an illustration of this for solitary waves overturning on plane slopes). It is important to note that, in numerical models, difficulties arise to compute accurately u_c and c for rapidly evolving breaking waves, and sometimes c is approximated by the shallow water linear wave phase velocity $\sqrt{gh}$. Experimental studies performed in deep water [25, 28, 29, 12] and shallow water [30] have found different thresholds for u_c/c, depending on the experimental configurations, ranging from 0.7 to 1.05.

1.3. Dynamic breaking criterion

Dynamic breaking criteria have been proposed in the last two decades, but mostly for deep water waves. Empirical findings based on observations of modulated deep water wave groups suggest that wave breaking occurs when the local wave energy flux within a group exceeds a given threshold [31]. These findings are supported by the experimental results of [32, 12] and [29]. [33] recently proposed, based on a numerical analysis of three-dimensional directionally focused wave packets in deep and intermediate water, a wave breaking onset criterion B_x based on the ratio of the local energy flux to the energy density, normalized by the local crest speed magnitude. At the free surface, this criterion reduces to $B_x = u_c/c$. [33] showed that if B_x exceeded the threshold $0.85 - 0.86$, wave breaking inevitably occurs within a fraction of a wave period. Thus, the threshold that they propose is not strictly speaking a breaking onset criterion, but is a

precursor to breaking onset criterion. Although their work is still ongoing, [34] recently reported that the same $B_x = 0.85 \pm 0.02$ criterion was able to predict similarly the eventual onset of wave breaking in shallow water conditions. The recent work of [35] confirms the validity of [33]'s breaking onset criterion for shallow water waves.

In the present work, based on numerical simulations with the 2D Fully Nonlinear Potential Flow (FNPF) model of [36], the validity of kinematic breaking onset criteria in shallow water is explored, and a new criterion is proposed that, for the waves studied here, improves breaking onset detection in comparison to the conventional kinematic criterion u_c/c.

The paper is organized as follows: in Section 2, the new breaking criterion is defined, and in Section 3 the model used in the study is introduced briefly. Comparisons between u_c/c and the new breaking criterion for different breaking wave conditions in shallow water are presented in Sections 4 to 6. Finally, conclusions are presented in Section 7.

2. Definition of a new kinematic breaking criterion

[25] studied the conventional u_c/c kinematic criterion using a variety of methods to compute the wave phase speed. However, they concluded that any of the methods they used, allowed to confirm the validity of this criterion. Here, the objective is instead to focus on the other parameter in the criterion, the surface fluid velocity. Numerical results presented hereafter will show, for a large range of incident wave conditions and sloping bottom geometries, that when breaking is initiated by wave overturning (i.e. for spilling and plunging breakers), the maximum fluid velocity at the surface $\|\mathbf{u}\|_m$, does not necessarily occur at the wave crest, but rather ahead of the crest on the front face. Breaking onset thus refers to the instant in time when part of the wave front face becomes vertical. It is thus possible to track more accurately the location where the instability leading to overturning of the wave crest develops (see Figure 3). This is consistent with the findings of [37] and [38] who found, based on PIV measurements of deep water spilling and plunging breakers, that the largest flow velocity occurs along the uppermost part of the wave front, but not necessarily at the crest itself. This observation led to investigate the skill of a new kinematic criterion at capturing wave breaking onset in shallow water, defined as:

$$\frac{\|\mathbf{u}\|_m}{c} \simeq 1. \tag{1}$$

In the following, the performance of the new criterion, defined in Equation (1), is compared to that of $u_c/c \simeq 1$ for capturing accurately wave breaking onset.

3. The FNPF model and some definitions

3.1. The FNPF model

Detailed characteristics of shoaling waves near and at the breaking point will be simulated with the FNPF model of [39] and [36] (hereafter referred to as 2D-NWT, i.e. 2D numerical wave tank), such as phase speed and particle velocities, and the performance of breaking onset criteria will be evaluated.

In the 2D-NWT, mass conservation is solved with a BEM using higher-order elements (at least cubic) ensuring local continuity of the first-derivatives of the geometry and field variables along the free surface. The nonlinear kinematic and dynamic free surface boundary conditions are time integrated using an explicit second-order Eulerian-Lagrangian scheme (this formalism was first proposed by [40]). An adaptive time step, based on a mesh Courant number, allows achieving accurate results when the distance between free surface nodes, here identical to Lagrangian particles, decreases. This typically occurs near and at the wave crests and subsequently within the tip of breaker jets. A summary of the model equations is presented in Appendix A, and more details about the mathematical model and numerical methods can be found in [39] and [36].

Models based on FNPF theory have been shown to predict accurately the wave shape geometry of wave shoaling up to and into the early stages of wave overturning, before touchdown of the breaker jet on the free surface (before blow-up of the model). [41, 42, 43] provide extensive validation of the wave geometry with the 2D-NWT for the simulation of shoaling and breaking of solitary waves over slopes and submerged breakwaters by comparing to laboratory data. [44], [45], and [20] provide similar results for regular waves. [27] has also used this 2D-NWT as a standard of accuracy to validate their fully-nonlinear Boussinesq-type wave model.

Since the wave geometry is accurately simulated by the model, at and into breaking, this indirectly validate the underlying parameters such as wave kinematics at and near the surface. Therefore, the 2D-NWT model can be used to gain physical insight into complex nonlinear wave phenomena such as breaking onset based on kinematic parameters. In the present computations, the accuracy of the numerical results will be assessed by verifying the global conservation of wave volume and total energy.

3.2. Computation of u_c/c and $\|\boldsymbol{u}\|_m/c$ in the 2D-NWT

Computing the breaking onset criteria, u_c/c and $\|\mathbf{u}\|_m/c$, at each time step of the 2D-NWT simulations requires calculating the horizontal fluid velocity at the wave crest, the maximum fluid velocity on the surface, and the wave phase speed.

According to potential flow theory, the fluid velocity is given by $\mathbf{u} = \nabla\phi$ (with ϕ the velocity potential), or in a local orthogonal coordinate system, tangential and normal to the free surface, as $\mathbf{u} = (u_s, u_n)$, with the normal velocity defined as $u_n = \partial\phi/\partial n$ and the tangential velocity as $u_s = \partial\phi/\partial s$. Since $(\phi, \partial\phi/\partial n)$ are the working variables of the 2D-NWT, they are computed at free surface nodes at each time step t of the simulation (using a cubic interpolation in between nodes). The tangential derivatives are then computed using a 5th-order sliding polynomial interpolation (see [36]). The horizontal velocity along the free surface is

found by projecting the local velocity components as $u = u_s \cos\beta + u_n \sin\beta$, with β the angle between the horizontal axis and the tangent to the free surface. At the wave crest, the latter is zero and thus $u_c = u_s$. Similarly, the velocity magnitude is computed as $\|\mathbf{u}\| = \sqrt{u_s^2 + u_n^2}$, and its maximum $\|\mathbf{u}\|_m$ is calculated as the upper bound of the local maximum within each boundary element close to the crest.

The phase speed c is known to be difficult to calculate accurately or to measure at arbitrary points of a non-permanent wave form [e.g. 27]. [25] compared three different definitions of phase speed from: (i) linear wave theory, (ii) a Hilbert transform, and (iii) the speed of a wave crest. Here, particularly since solitary waves are primarily considered, the speed of the wave crest (i.e. a local maximum in surface elevation) is used, which can be computed with a simple wave crest tracking method. Thus, in each simulation, the location of the maximum surface elevation, $x_c(t)$ is first calculated at each time t, using cubic interpolation in the BEM. Once model simulations are completed, a 4th-order polynomial is fit to the part of this time series including a short time before and after breaking onset, x_{cfit}, and the crest velocity (phase speed) is calculated analytically as $c = \mathrm{dx_{cfit}/dt}$ from this polynomial fit.

3.3. Breaking onset definition

The time of breaking onset is denoted by t_b and defined as the time when the wave front face becomes vertical within a boundary element (i.e. there is a vertical tangent with $\beta = \pi/2$). Although the cubic discretization will play a small role, for a fine discretization, this will also be approximately the time a free surface node overtakes another one in the wave propagation direction. Once this occurs, the free surface slope exceeds the vertical (i.e. $\beta > \pi/2$), and the wave overturns, passing a point of no return and starting to break. The comparison of the two kinematic breaking criteria, u_c/c and $\|\mathbf{u}\|_m/c$, will be done in the following applications based on this definition of breaking onset. It is interesting to note here that this particular definition of wave breaking onset may sometimes but not always correspond to other definitions, such as the wave reaching its maximum elevation.

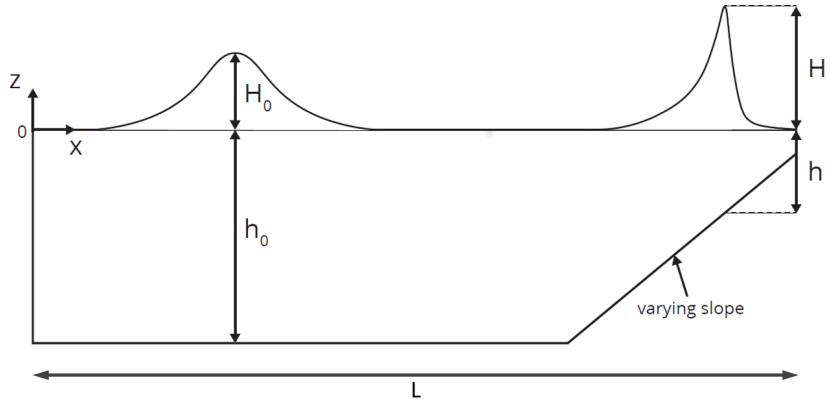

Figure 1: Definition sketch of numerical simulations with the 2D-NWT for solitary wave propagation over a plane slope.

4. Solitary wave propagating over a plane beach

The performance of the kinematic breaking criteria, u_c/c and $\|\mathbf{u}\|_m/c$ is first investigated with the 2D-NWT for a series of simulations of solitary wave shoaling and overturning over slopes (e.g. Figure 1). Although solitary waves are idealized limiting form (i.e. with an infinite wavelength and no trough), long waves that do not strictly occur in nature, many observations have shown that long and nonlinear shallow water swells can be approximated by a succession of solitary waves as they approach the shore, since they increasingly have steep and narrow crests separated by long shallow troughs [46]. A practical advantage of using solitary waves in FPNF models is that the computations are interrupted when a breaker jet impacts the free surface, which only occurs once per simulation with this type of wave.

Here, fully nonlinear solitary waves are specified as the initial condition in the constant depth (h_0) region of the computational domain (Figure 1) based on the numerically exact geometry and kinematics (potential ϕ, normal velocity $\partial\phi/\partial n$, and elevation η) computed with the method of [47]. This method provides the wave properties to an accuracy of at least 9 significant digits.

In the following, prime variables denote dimensionless variables where length is normalized by h_0 and time by $\sqrt{h_0/g}$.

Table 1: Physical parameters and numerical results for computations of solitary wave shoaling over a plane beach.

Simulations	s	H_0'	S_0	λ'	nd. per λ'	L'	u_c/c	$\|\mathbf{u}\|_m/c$	H_b/h_b
S100_H70	1:100	0.70	0.018	19.28	202	80.0	1.008	1.079	1.022
S100_H60*	1:100	0.60	0.020	20.24	212	80.0	0.995	1.074	1.036
S100_H50	1:100	0.50	0.022	21.52	184	98.0	0.994	1.064	1.043
S100_H40	1:100	0.40	0.024	23.16	198	98.0	0.996	1.071	1.048
S100_H30	1:100	0.30	0.028	25.8	188	115.0	1.016	1.085	1.049
S100_H20	1:100	0.20	0.034	30.47	222	115.0	1.006	1.028	1.058
S050_H60	1:50	0.60	0.039	20.17	260	80.0	0.992	1.084	1.181
S050_H40	1:50	0.40	0.048	30.32	348	80.0	0.988	1.087	1.259
S050_H20	1:50	0.20	0.068	30.36	318	80.0	0.995	1.072	1.257
S035_H60	1:35	0.60	0.056	20.16	328	51.5	0.978	1.081	1.314
S035_H40	1:35	0.40	0.069	23.17	292	66.5	0.966	1.079	1.373
S035_H30	1:35	0.30	0.079	25.87	326	66.5	0.968	1.085	1.407
S035_H20	1:35	0.20	0.097	30.31	382	66.5	0.977	1.101	1.462
S020_H70	1:20	0.70	0.091	19.23	424	38.0	0.914	1.026	1.649
S020_H60	1:20	0.60	0.098	20.22	446	38.0	0.922	1.046	1.724
S020_H50	1:20	0.50	0.108	51.41	390	46.0	0.931	1.061	1.792
S020_H40	1:20	0.40	0.120	23.16	422	46.0	0.934	1.073	1.870
S020_H20	1:20	0.20	0.170	30.23	478	53.0	0.892	1.046	2.180
S015_H60	1:15	0.60	0.131	20.18	376	44.985	0.869	1.003	2.176
S015_H50	1:15	0.50	0.143	21.47	400	44.985	0.868	1.012	2.296
S015_H40*	1:15	0.40	0.160	23.19	432	44.985	0.866	1.018	2.441
S015_H30	1:15	0.30	0.185	25.77	480	44.985	0.845	1.007	2.669

*Simulations appearing in Figure 3

4.1. Model parameters

The computational domain used to simulate solitary wave shoaling and overturning is shown in Figure 1. The length of the domain L' is function of the plane slope s = 1:100 to 1:15 and the initial equivalent length of the solitary wave λ' (see Table 1). Solitary waves of model input initial height $H'_0 = 0.2$ to 0.7 were simulated with each solitary wave generated such that its minimum surface elevation is a given fraction $\varepsilon_z = 0.001$ of its maximum elevation H'_0, which yields the value of the equivalent length λ' (note that λ' is also a weak function of the free surface discretization and domain geometry, so λ' varies slightly for the same incident waves propagating over different slopes). Hence, the computational domain is longer for smaller incident waves (smaller solitary waves are longer) and milder slopes. Initial wave heights and slopes are combined to create 22 test cases of different types of wave breaking. Both the physical and numerical parameters for each of these test cases are listed in Table 1. Following [43], the corresponding surf-similarity parameter, $S_0 = 1.521 s/\sqrt{H'_0}$ of these solitary waves ranges from 0.018 to 0.185, indicating spilling ($S_0 < 0.025$) or plunging ($0.025 < S_0 < 0.30$) wave breaking.

The BEM computational domain boundary is discretized with N nodes, including N_f nodes on the free surface. To increase the accuracy of the simulations, the latter is a large fraction of N (typically over 80%, see below). Because the domain length and wavelength vary, the number of nodes per wave length (nd. per λ) is different in each simulation. So-called cubic "Mid-Interval-Interpolation" (MII) boundary elements are used to interpolate the solution in between nodes on the free surface, and 3-node quadratic isoparametric elements on other parts of the boundary (see [36]). The bottom discretization is typically much coarser than the free surface discretization, but to increase accuracy in shallower water, the discretization is non-uniform over the slope with the distance between nodes decreasing gradually with the depth. Consistent with the Eulerian-Lagrangian formalism, the BEM nodes on the free surface gradually converge near the crest region during the shoaling phase preceding breaking onset, which also increases the accuracy of the results in shallower water.

A convergence study as a function of the discretization, detailed in Appendix B, was first performed to establish the minimum discretization required to ensure both accurate and converged results, particularly for the parameters of interest (flow velocity and phase speed) at breaking onset. Shoaling of a solitary wave with $H'_0 = 0.6$ was simulated over 1:15 and 1:100 slopes, and maximum relative errors of the solitary wave volume and total energy (as compared to initial values computed with the method of [47]) were computed, together with the values of u_c/c, $\|\mathbf{u}\|_m/c$, and c at breaking onset. Nine different discretizations were tested for each case and it was found that using $N = 1038$ and $N_f = 838$ ensured that both errors remained smaller than 0.01% while the values of the breaking onset parameters had clearly converged to within less than 0.2% at least three configurations coarser than the selected one ($N = 1038$ and $N_f = 838$). These values of N and N_f were thus used in the 22 test cases studied here, with the model parameters and results shown in Table 1. [Note that in this table H_b and h_b denote the breaking wave height (crest elevation for a solitary wave) and water depth, respectively, and $\gamma = H_b/h_b$ is the breaker index, at t_b.]

To assess further the accuracy of the numerical results for these cases, the maximum relative errors of wave volume and energy conservation were also calculated up to breaking onset. Figure 2 shows the maximum absolute errors of wave energy $\|\varepsilon_e\|$ and volume $\|\varepsilon_v\|$, calculated for wave propagation from $t = 0$ to t_b. At most, the maximum error for energy reaches 0.2% and for volume 0.015%, which is sufficient to ensure reliable estimates of the breaking onset parameters (u_c, $\|\mathbf{u}\|_m$, c) based on the convergence study in Appendix B. [Note that this convergence study also showed that the breaking onset parameters converged for coarser discretizations (and hence for larger numerical errors) than achieved with this discretization.]

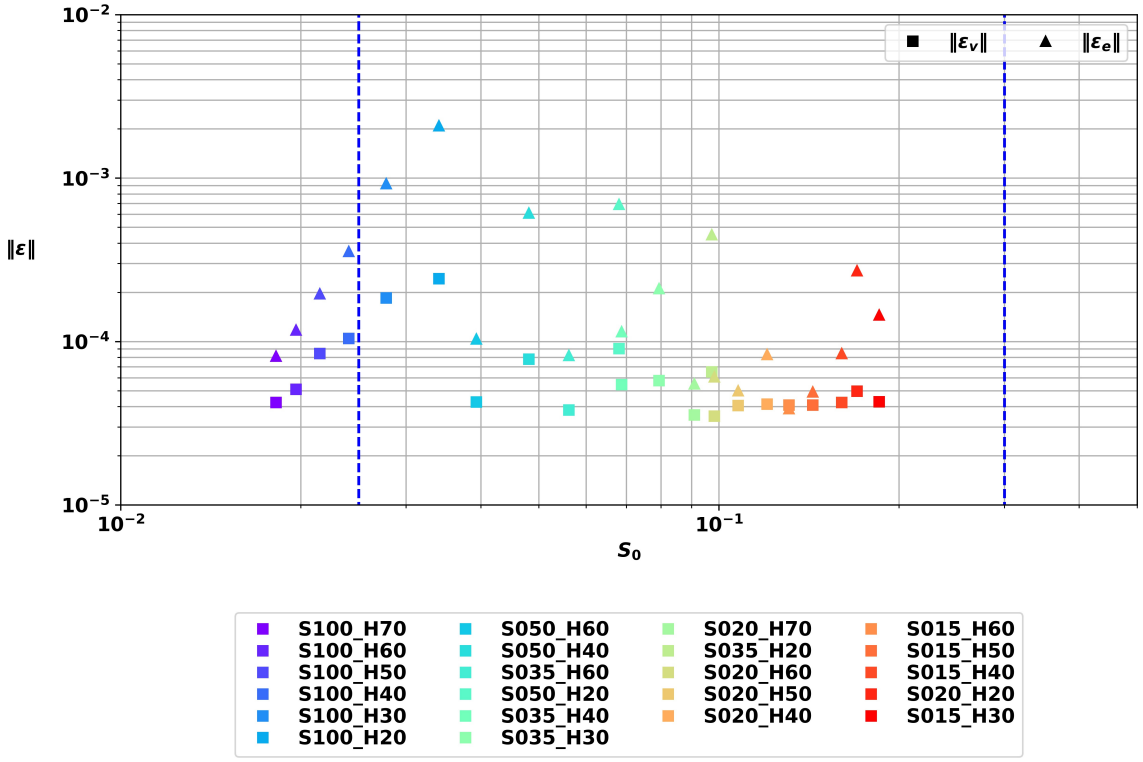

Figure 2: Absolute maximum numerical errors with respect to initial values computed with the method of [47], as a function of S_0 for the wave volume $\|\varepsilon_v\|$ and total energy $\|\varepsilon_e\|$.

4.2. Comparison of u_c/c and $\|\boldsymbol{u}\|_m/c$ breaking onset criteria

Some of the solitary wave cases simulated in this study (parameters listed in Table 1) were similar to the cases modeled and analyzed by [43]. Additional simulations were performed for different slopes (e.g. 1:20 and 1:50) and incident wave heights. Figure 3 shows the free surface elevation simulated with the 2D-NWT at four different time steps (with the second being t_b) for a mild spilling breaker (top panel $H_0' = 0.6$ on a 1:100 slope) and for a more intense plunging breaker (bottom panel, $H_0' = 0.4$ on a 1:15 slope). The symbols on each free surface profile mark the location of the maximum elevation (i.e. wave crest) and that of the maximum velocity $\|\mathbf{u}\|_m$. They are in general different, although they are much closer for the spilling breaker than for the plunging breaker. At t_b, $\|\mathbf{u}\|_m$ occurs approximately at the location where the wave front face is vertical and a breaker jet will soon be emerging, leading to wave overturning.

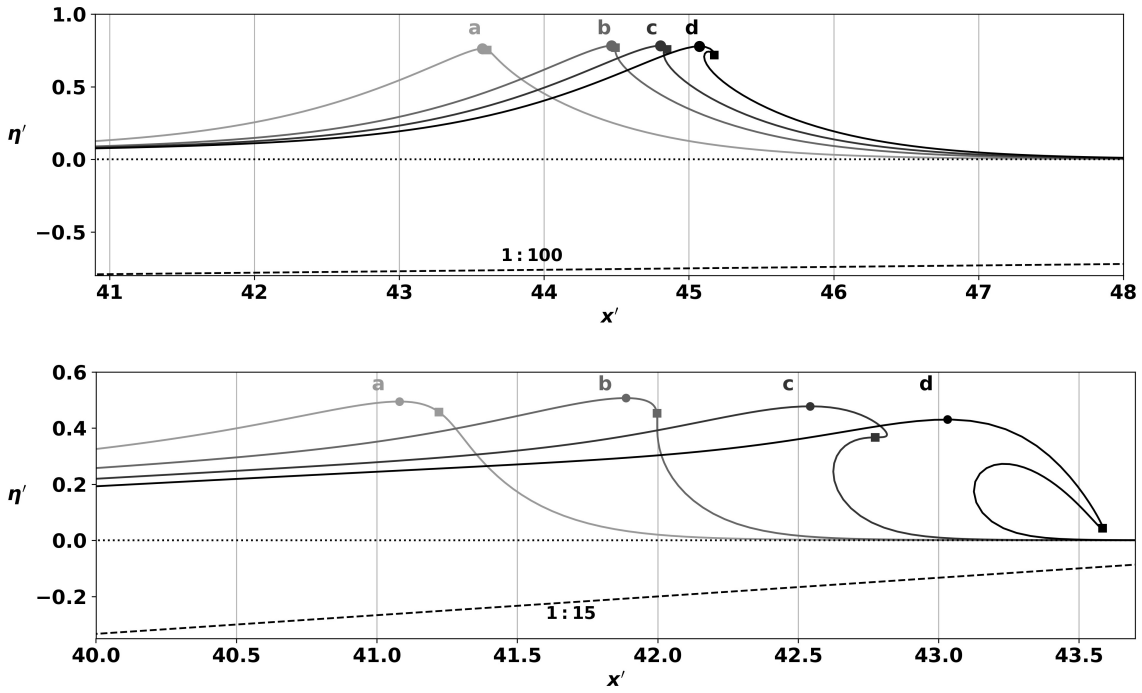

Figure 3: Solitary wave propagation simulated with the 2D-NWT up to overturning of the wave crest for: (top panel, spilling breaker) a wave with an initial height $H'_0 = 0.6$ over a 1:100 slope, and (bottom panel, plunging breaker) a wave with an initial height $H'_0 = 0.4$ over a 1:15 slope. Curves a,b,c,d are results obtained for increasing times (discussed in the text). In each case, curve b corresponds to the breaking onset time t_b, at which the front face of the wave becomes vertical. The locations of the crest (maximum elevation) and maximum velocity $\|\mathbf{u}\|_m$ are marked by circle and square symbols, respectively.

Figure 4 shows the breaking onset parameter values u_c/c and $\|\mathbf{u}\|_m/c$ computed for each case in Table 1, either as a function of time $t'-t'_b$, or at $t' = t'_b$ as a function of S_0. Both u_c/c and $\|\mathbf{u}\|_m/c$ increase continuously with time and, because the maximum fluid velocity is larger than the horizontal velocity at the crest, $\|\mathbf{u}\|_m/c$ reaches larger values at t'_b than u_c/c. Figures 4 (b) and (d) show that at breaking onset, $u_c/c \in [0.845-1.015]$ while $\|u\|_m/c \in [1.003-1.101]$. More specifically, u_c/c value at breaking onset decreases with an increasing S_0. For only spilling breakers and small plunging breakers (i.e. $S_0 < 0.8$), the 95% confidence interval of u_c/c is $u_c/c = 0.992 \pm 0.028$ at breaking onset, but this value becomes much smaller for intense plunging breakers, $u_c/c = 0.902 \pm 0.075$. Considering all test cases, $u_c/c = 0.951 \pm 0.104$. In contrast, the corresponding 95% confidence interval of $\|\mathbf{u}\|_m/c$ values at breaking onset is narrower, with $\|\mathbf{u}\|_m/c \simeq 1.058 \pm 0.057$ for all the cases in Table 1, which provides a good prediction of breaking onset even for strong plunging waves.

This figure highlights two significant findings. First, consistent with the work of [35] it shows that the results of [33] can be extended to shallow water: the parameter $B_x = u_c/c \approx 0.85$ is thus an accurate universal precursor to breaking initiation. Second, $\|\mathbf{u}\|_m/c$ also agrees with this finding and is even closer to $\|\mathbf{u}\|_m/c \approx 1$ at breaking initiation, which likely results from $\|\mathbf{u}\|_m$ capturing better the location where overturning starts as compared to u_c.

Finally, the differences between $\|\mathbf{u}\|_m$ and the maximum horizontal particle velocity u_m on the free surface (not detailed in the paper) showed that u_m and $\|\mathbf{u}\|_m$ are almost identical until breaking, as the vertical

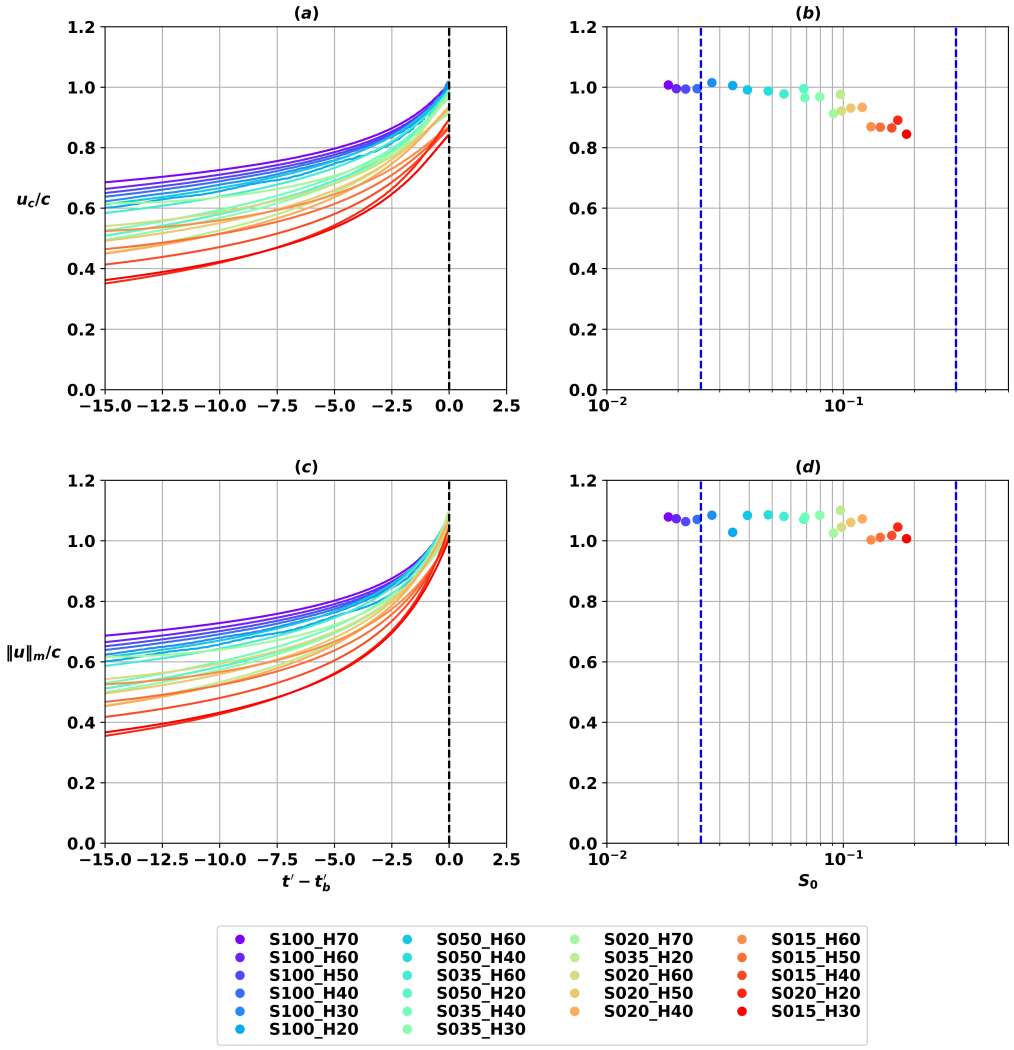

Figure 4: Computations of solitary wave shoaling and overturning over a plane slope. Breaking onset criteria computed: (a,c) as a function of $t' - t'_b$ and (b,d) at t'_b as a function of the surf-similarity parameter S_0. Each breaking wave is identified by a color and label identical to those listed in Table 1, which shows the related parameters values and results. Labels indicate both slope and wave height with, for example, S020_H70 referring to a wave with $H'_0 = 0.70$ propagating over a 1:20 slope.

component of the free surface velocity w is very small in the crest area. Then $\|\mathbf{u}\|_m$ becomes larger than u_m a short time before breaking, particularly for plunging breakers, and the difference between these velocities continues to increase beyond breaking onset.

5. Solitary wave propagating over a submerged bar

In this application, the variation of u_c/c and $\|\mathbf{u}\|_m/c$ is investigated for solitary waves shoaling over a submerged bar with a 1:20 front slope, a crest at $0.75h_0$, and a 1:10 back slope. The bar crest length is $5h_0$ (see Figure 5). [48] first proposed this bar geometry and used it to perform both laboratory experiments and numerical simulations of regular wave shoaling and energy transfers between higher-order harmonics. [20] validated the 2D-NWT with measurements from several of the test cases in these experiments. The present

study uses the same bar geometry but instead evaluates the properties of breaking solitary waves propagating over the bar.

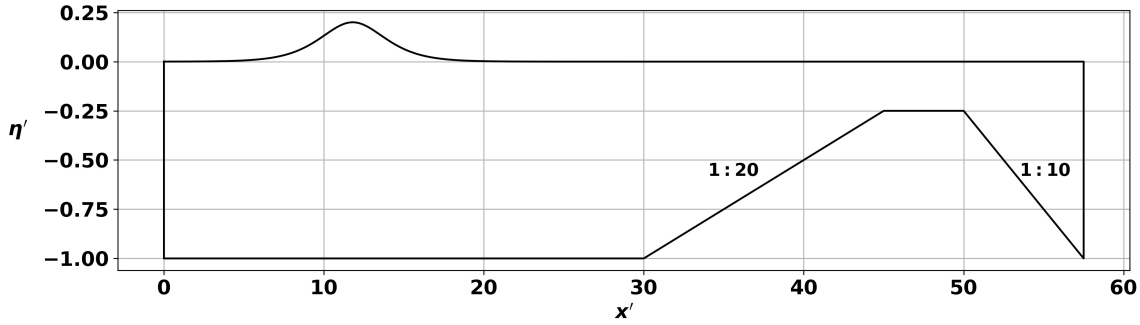

Figure 5: Computational domain used in 2D-NWT simulations of solitary wave propagating over a submerged bar.

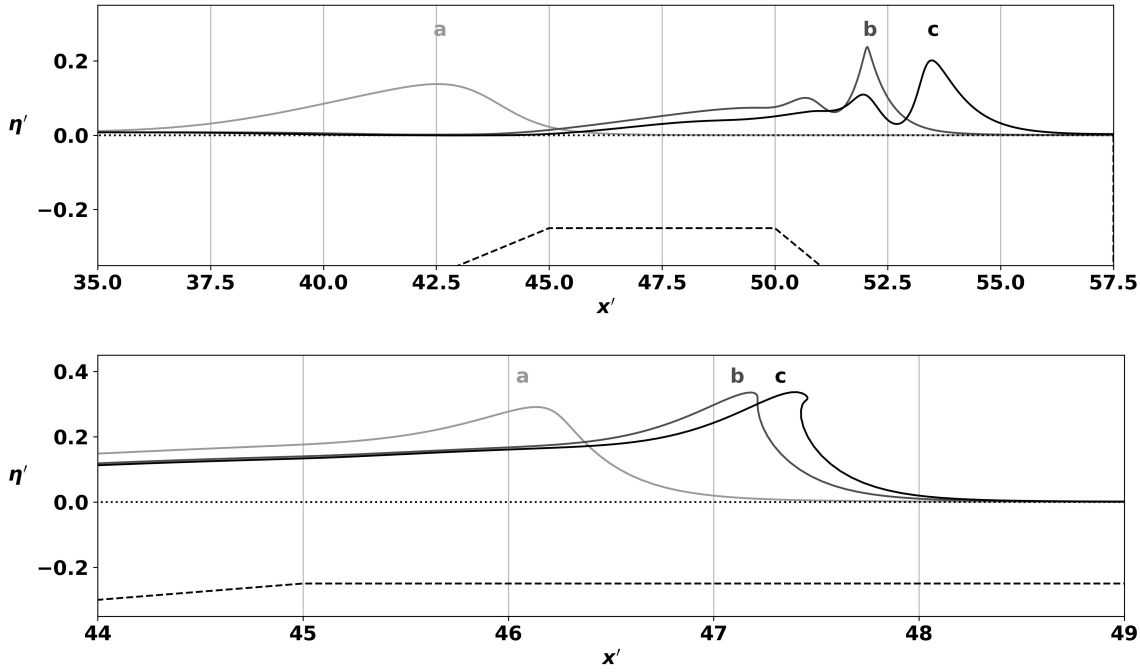

Figure 6: Simulated free surface elevation of solitary waves propagating over a submerged bar: (top panel) $H_0' = 0.1165$ (non-breaking case) and (bottom panel) $H_0' = 0.2$ (breaking case). Curves a,b,c represent different time steps. In the top panel, curve b corresponds to the time the crest reaches its maximum elevation, while in the bottom panel curve b corresponds to $t = t_b$, i.e. breaking onset.

5.1. Model parameters

Table 2 provides physical and model parameters for the simulated test cases, as well as numerical results of the estimated breaking onset parameter values. Figure 5 shows the computational domain used in the 2D-NWT. Here, to reduce the computational effort, the domain is truncated, with a vertical wall specified at the toe of the bar back slope ($x' = 57.5$). The computations were stopped before any reflections from the far end of the 2D-NWT could propagate back into the area of interest over the bar. The model input wave height in the different test cases varied from $H_0' = 0.1106$ to 0.3, with corresponding incident equivalent

Table 2: Physical parameters and numerical results for computations of solitary waves propagating over a submerged bar. The domain length is $L' = 57.5$ in all cases.

Simulations	H'_0	λ'	nd. per λ'	u_c/c	$\|\mathbf{u}\|_m/c$	Breaking	H_b/h_b
HBS1160	0.1106	29.78	434	0.776	0.782	No	0.52
HBS1165*	0.1165	29.78	434	0.793	0.801	No	0.52
HBS1170	0.1170	29.64	432	0.826	0.834	No	0.53
HBS1175	0.1175	29.64	432	0.874	1.016	Yes	0.51
HBS1500	0.15	26.62	388	1.080	1.006	Yes	1.17
HBS2000*	0.2	23.60	344	0.926	1.050	Yes	1.34
HBS2500	0.25	21.55	314	0.885	1.025	Yes	1.53
HBS3000	0.3	20.04	292	0.923	1.067	Yes	1.74

*Simulations appearing in Figure 6

wavelengths varying from $\lambda' = 20.04$ to 29.78. The BEM discretization for this case was selected following the same approach as for the previous application with a plane slope. The number of nodes per wavelength varies from 292 to 434 on the free surface.

In this application, both breaking and nearly breaking solitary waves are simulated. For the latter, the waves shoal and nearly reach breaking onset over the bar crest, but do not break and continue propagating beyond the bar. With this bar geometry, numerical experiments showed that incident solitary waves with $H'_0 < 0.1175$ did not break (e.g. Figure 6, top panel), whereas those with a larger incident wave heights did break (e.g. Figure 6, bottom panel).

5.2. Comparison of u_c/c and $\|\boldsymbol{u}\|_m/c$ breaking onset criteria

Figure 7 compares the breaking onset parameter values u_c/c and $\|\mathbf{u}\|_m/c$ computed for each case in Table 2, either as a function of time $t' - t'_b$, or at $t' = t'_b$ as a function of H'_0. For non-breaking cases, the reference time used (instead of t_b) corresponds to the time the crest reaches its maximum elevation. Figure 7 (a) shows that the conventional breaking onset criterion $u_c/c \simeq 1$ does not allow distinguishing between breaking and non-breaking waves. Further, consistent with the findings of [33] and [35], Figure 7 (b) shows that only waves for which u_c/c becomes larger than 0.85 during shoaling on the bar will evolve towards breaking (see also Table 2). In Figures 7 (c) and (d), this appears to apply to $\|\mathbf{u}\|_m/c$ as well, which remains below 0.85 for non-breaking waves. This is likely because the location of $\|\mathbf{u}\|_m$ is very close to the crest for the considered waves, hence $\|\mathbf{u}\|_m \simeq u_c$ for waves that do not evolve towards breaking. In contrast, for breaking wave cases, the 95% confidence intervals are computed as $u_c/c \simeq 0.906 \pm 0.044$ and $\|\mathbf{u}\|_m/c \simeq 1.032 \pm 0.044$ at t_b. Therefore, while $u_c/c \approx 0.85$ allows to distinguish breaking from non-breaking cases, this difference appears to be more pronounced with $\|\mathbf{u}\|_m/c \simeq 1$.

6. Quasi-regular wave propagating over a submerged bar

Finally, the shoaling of quasi-regular waves over the same submerged bar as in the previous application is simulated to assess whether the same conclusions apply regarding the breaking onset criteria. Running

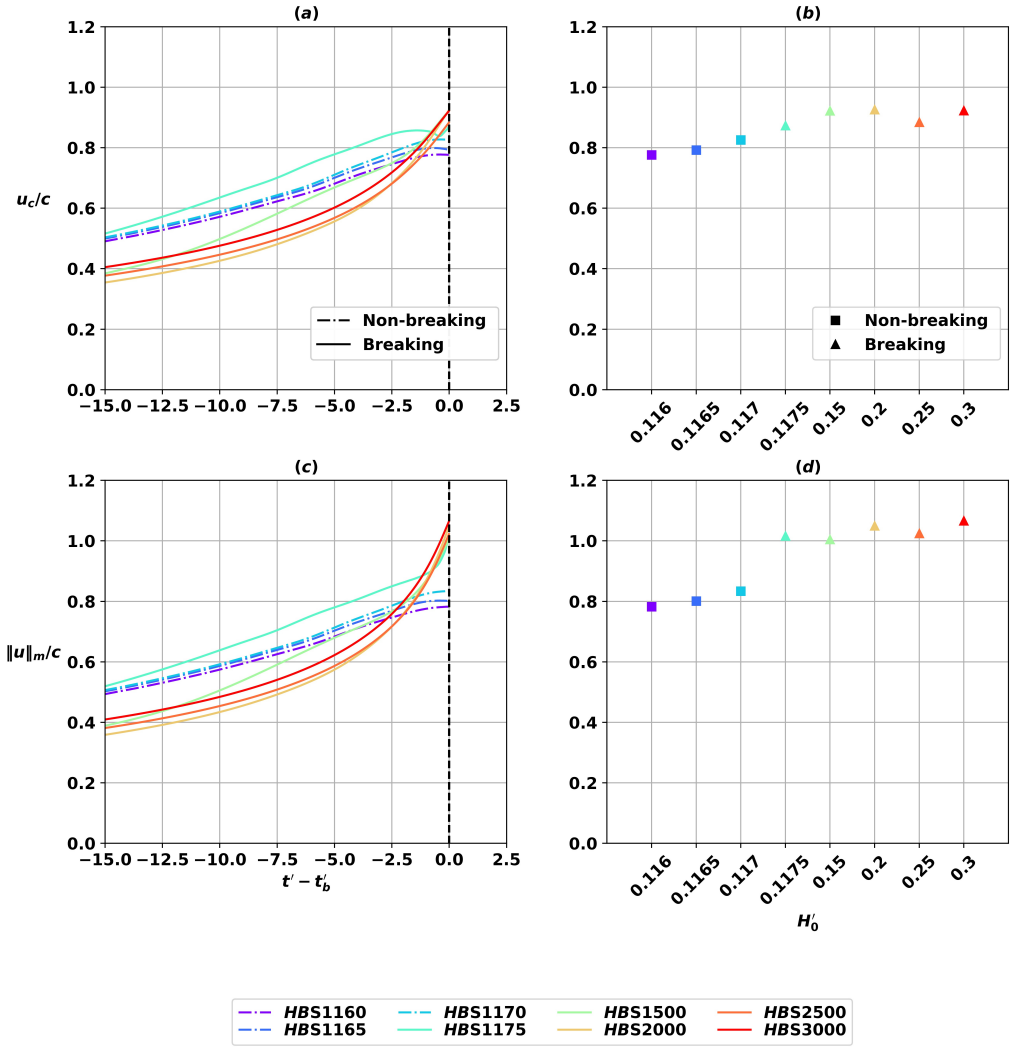

Figure 7: Breaking onset criteria computed for the solitary waves propagating over a submerged bar: (a,c) as a function of $t' - t'_b$ and (b,d) at t'_b as a function of H'_0. Each wave is identified by a color and a label identical to those listed in Table 2, which shows the related parameters values and results. Note, for the non-breaking cases, the reference time used (instead of t_b) corresponds to the time the crest reaches its maximum elevation.

simulations with quasi-regular (or even irregular) waves in the 2D-NWT is possible, but becomes more computationally expensive.

6.1. Model parameters

The physical and model parameters for the simulated test cases are shown in Table 3. Figure 8 shows the computational domain used in the 2D-NWT. As compared to the previous computational domain used to propagate and shoal solitary waves, the length of the constant depth region offshore of the bar is reduced such that the toe of the bar back slope is now at $x' = 42.5$, and then an absorbing beach (AB) of length $l'_{AB} = 20$ is specified to minimize reflections from the far-end of the 2D-NWT (see [44] for more details). Numerically exact FNPF regular waves are generated on the offshore boundary, as "zero-mass-flux" stream function waves (see [44] for more details). The model input wave period is $T' = 4$ in all cases, and the model

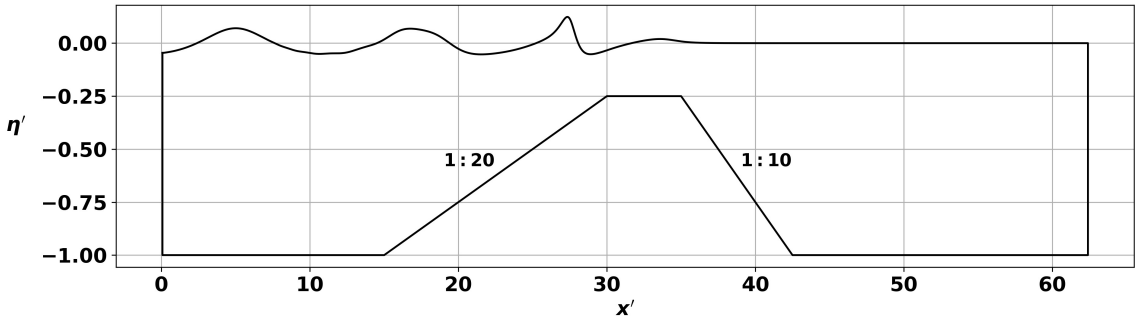

Figure 8: Computational domain used in 2D-NWT simulations of quasi-regular wave propagating over a submerged bar. An absorbing beach of length l'_{AB} is specified at the far-end of the domain, starting at $x' = 42.5$.

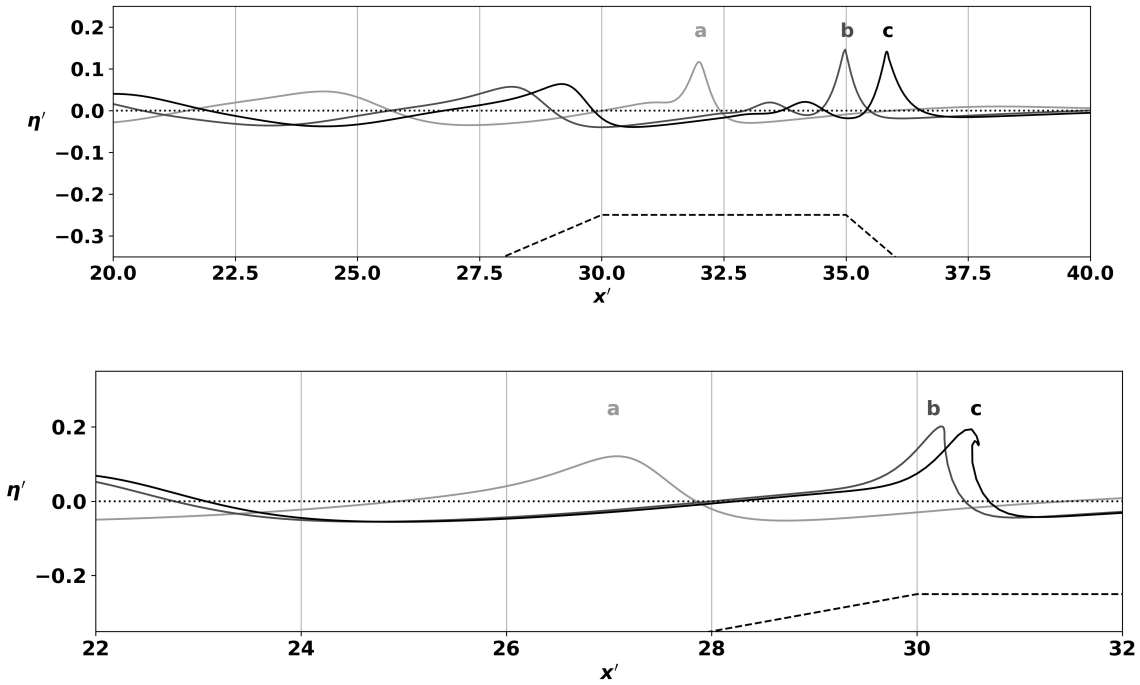

Figure 9: Simulated free surface elevations for quasi-regular waves of period $T' = 4$ shoaling over a submerged bar: (top panel) $H'_0 = 0.065$ (non-breaking case) and (bottom panel) $H'_0 = 0.12$ (breaking case). Curves a,b,c represent different time steps. In the top panel, curve b corresponds to the time the crest reaches its maximum elevation, while in the bottom panel curve b corresponds to $t = t_b$, i.e. the time of breaking onset.

input wave height is varied from $H'_0 = 0.06$ to 0.2 with an incident wavelength of approximately $\lambda' = 12$. The BEM discretization was selected following the same approach as in previous applications. The number of nodes per wavelength is approximately 160 on the free surface. Since the 2D-NWT simulation is terminated once a breaker jet impacts the free surface, a fully stationary regular wave train can not be achieved. In the following, we will therefore only study the first breaking wave in the wave train, which is thus quasi-regular and not purely regular for the reasons explained above.

Both breaking and nearly breaking waves are investigated. For the non-breaking cases, only the first wave of the quasi-regular wave train is studied for consistency with the breaking cases. Numerical experiments showed that, for this bar geometry, incident regular parameters with $H'_0 < 0.0708$ (H'_0 is the input parameter

of the model) did not break (e.g. Figure 9 top panel), whereas those with a larger incident wave heights did break (e.g. Figure 9 bottom panel).

Table 3: Physical parameters and numerical results for computations of regular waves propagating over a submerged bar(Figure 5). The wave period is $T' = T/\sqrt{g/h_0} = 4$ and the domain length is $L' = 62.4$ for all cases.

Simulations	H'_0	λ'	nd. per λ	u_c/c	$\|\mathbf{u}\|_m/c$	Breaking	H_b/h_b
HBR0600	0.060	12.00	161	0.460	0.460	No	0.41
HBR0650*	0.065	12.00	161	0.552	0.553	No	0.48
HBR0700	0.070	12.00	161	0.751	0.763	No	0.58
HBR0708	0.0708	12.00	161	1.092	1.100	Yes	0.64
HBR0900	0.090	12.02	161	0.942	1.062	Yes	0.69
HBR1200*	0.12	12.05	162	0.861	0.999	Yes	0.81
HBR1500	0.15	12.10	162	0.863	0.984	Yes	0.84
HBR2000	0.2	12.18	163	0.873	0.989	Yes	0.84

*Simulations appearing in Figure 9

6.2. Comparison of u_c/c and $\|\boldsymbol{u}\|_m/c$ breaking onset criteria

Figure 10 compares the breaking onset parameter values u_c/c and $\|\mathbf{u}\|_m/c$ computed for each case in Table 3, either as a function of time $t' - t'_b$, or at $t' = t'_b$ as a function of H'_0. As in the previous section, for non-breaking cases, the reference time used (instead of t_b) corresponds to the time the crest reaches its maximum elevation. The evolution of the wave breaking onset criteria is recorded for the first wave of the wave train, in each case.

Similar to solitary waves, Figures 10 (a) and (b) show that the conventional breaking onset criterion $u_c/c \simeq 1$ does not allow distinguishing between breaking and non-breaking waves. Consistent with the findings of [33] and [35], Figures 10 (b) and (d) show that only waves for which u_c/c or $\|\mathbf{u}\|_m/c$ become larger than 0.85 during shoaling over the bar will evolve towards breaking (see also Table 3). For breaking wave cases, the 95% confidence intervals are wider than for solitary waves, $u_c/c \simeq 0.926 \pm 0.173$ and $\|\mathbf{u}\|_m/c \simeq 1.027 \pm 0.09$ at t_b. $\|\mathbf{u}\|_m/c$ is closer to a constant value than u_c/c.

7. Discussion and conclusions

In this study, numerical simulations were performed with a 2D-NWT to assess the ability of two kinematic breaking criteria u_c/c and $\|\mathbf{u}\|_m/c$ to predict correctly wave breaking onset for solitary and quasi-regular waves shoaling and breaking as spilling or plunging breakers over plane slopes or a mildly sloping bar.

The two breaking criteria only differ in the definition of the fluid velocity considered at the free surface: the first criteria u_c/c uses the horizontal component of the fluid velocity at the wave crest, while the second criteria $\|\mathbf{u}\|_m/c$ uses the maximum fluid velocity on the front face of the wave. These two velocities are usually quite similar up to close to breaking onset, but may then differ significantly. Here, the results show that the maximum velocity at the free surface occurs closer to the location of the initiation of the overturning jet than the wave crest (i.e. maximum elevation). This finding, which is supported by some experimental

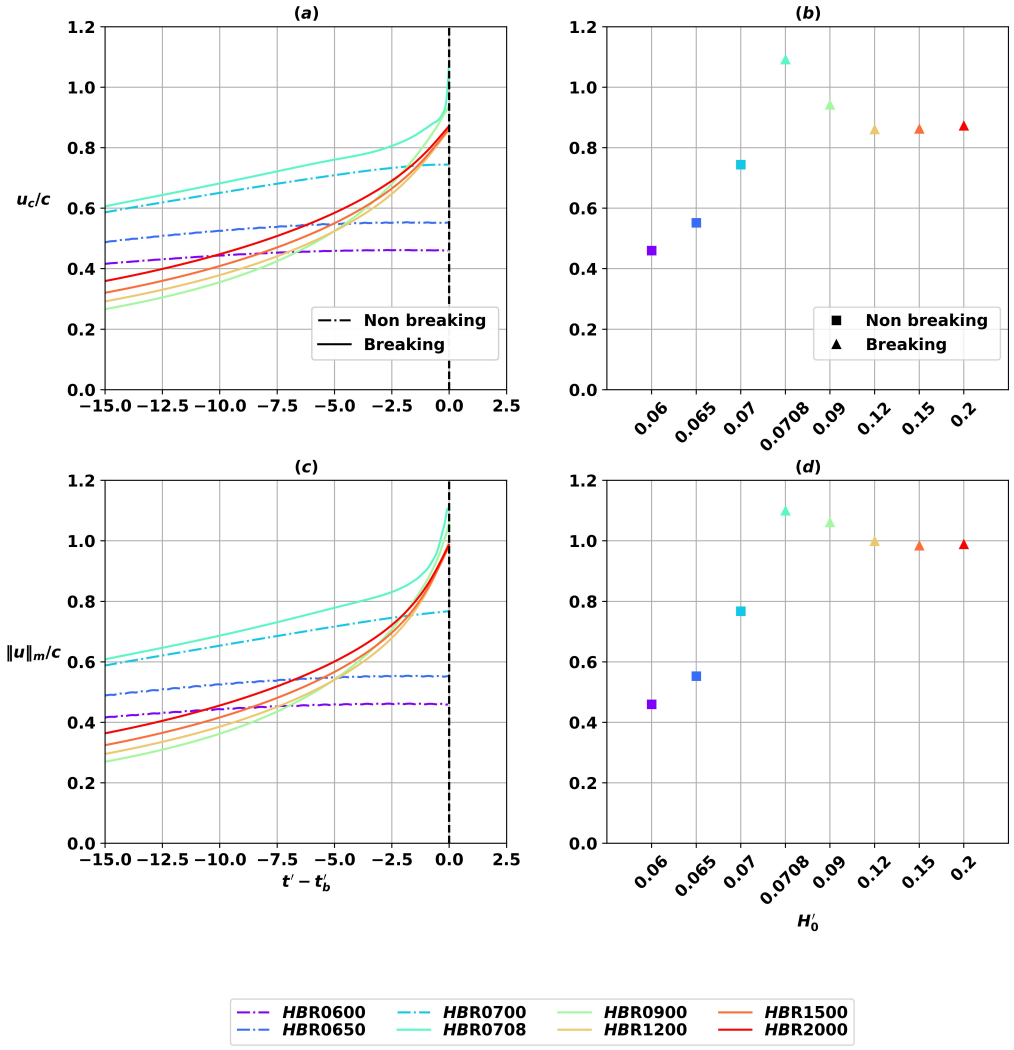

Figure 10: Breaking onset criteria computed for the first wave in the wave train of regular waves (period $T' = 4$) propagating over a submerged bar: (a,c) as a function of $t' - t'_b$ and (b,d) at t'_b as a function of H'_0. Each case is identified by a color and a label identical to those listed in Table 3, which shows the related parameters values and results. Note, for the non-breaking cases, the reference time used (instead of t_b) corresponds to the time the crest reaches its maximum elevation.

studies [37, 38], motivated the present investigation of the performance of the $\|\mathbf{u}\|_m/c$ criterion in capturing the onset of wave breaking.

In the configurations considered in this paper, including the propagation of solitary waves over a plane beach, and of solitary and quasi-regular waves over a submerged bar, $\|\mathbf{u}\|_m/c$ was found to predict the breaking onset with a higher accuracy than u_c/c, which varied over a wider range. Considering all the results summarized in Tables 1 to 3, the Root-Mean-Square (RMS) errors have been computed and they are minimized considering the empirical thresholds 0.95 and 1.05 for u_c/c and $\|\mathbf{u}\|_m/c$ respectively. The RMS errors are then 6.3 and 3.2%, with respect to $u_c/c = 0.95$ and $\|\mathbf{u}\|_m/c = 1.05$, respectively. Besides this improvement in terms of RMS errors, the results here suggest that the initiation of overturning for spilling or plunging breakers is captured more accurately when considering the location along the free surface of the

maximum fluid velocity.

These findings may help explain the scatter observed in breaking thresholds reported in the literature for kinematic breaking criteria based on the horizontal fluid velocity at the crest [e.g. 25, 28, 29, 12, 49]. However, the results presented here also showed that using u_c in the criteria is acceptable when considering the onset of spilling and small plunging breakers. For these cases, u_c/c is indeed close to 1 since the breaker jet forms close to the crest location. In contrast, for strong plunging breakers, $u_c/c < 1$ at breaking onset, since u_c underestimates the velocity representative of the breaker jet. In such cases, the plunging jet forms farther from the crest location. Therefore, the new kinematic criterion based on the maximum velocity observed along the free surface may be more universal, allowing improvements in the prediction of breaking onset for both spilling and plunging wave breaking. In all of the cases of breaking and non-breaking waves presented here, the results are consistent with the conclusions of [33] that waves with $B_x = u_c/c > 0.855 \pm 0.005$ will inevitably evolve towards breaking. This also appears to apply to $\|\mathbf{u}\|_m/c$.

This work demonstrates that $\|\mathbf{u}\|_m/c \approx 1$ can be used as a robust and accurate breaking onset criterion for identifying the initiation of breaking for both solitary and quasi-regular breaking waves in shallow water conditions.

Seiffert et al. [50] successfully implemented [33]'s criterion in a FNPF-HOS (High Order Simulation) model, which supports the practical applicability of our proposed new definition of the kinematic criterion to phase-resolving wave models, provided there is an additional step in the computations, to identify $\|\mathbf{u}\|_m$. Using this criterion rather than B_x may thus allow achieving a higher nonlinearity before dissipation is triggered in fully nonlinear wave models.

Note, however, that the validity of $\|\mathbf{u}\|_m/c$ in deep water conditions and for irregular and 3D waves has not yet been assessed. Grilli et al. [43] have shown that there exists self-similarity of breaking geometries and properties, indicating a "local loss of memory" of the flow for the phenomenon that has caused breaking, suggesting that whether the pre-breaking waves are solitary, quasi-regular, or even irregular should not significantly affect flow velocities at breaking onset the breaking crest. Still, rigorous validation of our new definition of the kinematic criterion in other situations would require further research.

Acknowledgments

This work has been done in the framework of the DiMe and CARAVELE projects, which benefit from French government support managed by the Agence Nationale de la Recherche (ANR) under the program "Investissement d'Avenir" ANR-10-IEED-0006-14 and ANR-10-IEED-0006-26. The numerical simulations were performed on the High Performance Computing (HPC) cluster Datarmor of the "Pôle de Calcul Intensif pour la Mer" (PCIM) (http://www.ifremer.fr/pcim). Volker Roeber acknowledges financial support from the Isite program Energy & Environment Solutions (E2S), the Communauté d'Agglomération Pays Basque (CAPB) and the Communauté Région Nouvelle Aquitaine (CRNA) for the chair position HPC-Waves.

Appendix A. Summary of the numerical model governing equations and numerical implementation

The velocity potential $\phi(x,t)$ is used to represent inviscid irrotational 2D flows in the vertical plane (x,z), and the velocity is defined by $\mathbf{u} = \boldsymbol{\nabla}\phi = (u,w)$. The continuity equation in the fluid domain $\Omega(t)$ with boundary $\Gamma(t)$ is the Laplace equation for the potential:

$$\boldsymbol{\nabla}^2\phi = 0 \qquad \text{in } \Omega(t) \tag{A.1}$$

The 2D-NWT model simulates 2D free-surface flows of an ideal fluid. Under such conditions, Green's second identity (with free space Green's function $G(\mathbf{x},\mathbf{x}_l) = -(1/2\pi)\log|\,\mathbf{x}-\mathbf{x}_l\,|$) makes it possible to transform the continuity equation for the velocity potential into a boundary-integral equation (BIE).

$$\alpha(\mathbf{x}_l)\phi(\mathbf{x}_l) = \int_{\Gamma(\mathbf{x})}\left[\frac{\partial\phi}{\partial n}(\mathbf{x})G(\mathbf{x},\mathbf{x}_l) - \phi(\boldsymbol{x})\frac{\partial G(\mathbf{x},\mathbf{x}_l)}{\partial n}\right]d\Gamma(\boldsymbol{x}) \tag{A.2}$$

in which $\mathbf{x} = (x,z)$ and $\mathbf{x}_l = (x_l,z_l)$ are position vectors for points on the boundary, $\mathbf{n}$ is the unit outward normal vector, and $\alpha(\mathbf{x}_l)$ is a geometric coefficient. Equation A.2 is solved by a BEM using a set of collocation nodes on the boundary and high-order elements to interpolate in between the collocation nodes. Integrals in A.2 are evaluated numerically, and the resulting algebraic system of equations is assembled and solved for the equivalent discretized problem. On the free surface $\Gamma_f(t)$, ϕ satisfies the nonlinear kinematic and dynamic boundary conditions,

$$\frac{D\mathbf{r}}{Dt} = \mathbf{u} = \nabla\phi \qquad \text{on } \Gamma_f(t) \tag{A.3}$$

$$\frac{D\phi}{Dt} = -gz + \frac{1}{2}\boldsymbol{\nabla}\phi\cdot\boldsymbol{\nabla}\phi - \frac{p_a}{\rho} \qquad \text{on } \Gamma_f(t) \tag{A.4}$$

respectively, with $\mathbf{r}$ the position vector of a free surface fluid particle, g the acceleration of gravity, z the vertical coordinate (positive upwards, with $z=0$ at the undisturbed free surface), p_a the atmospheric pressure, ρ the fluid density, and the material derivative being defined as,

$$\frac{D}{Dt} \equiv \frac{\partial}{\partial t} + \mathbf{u}\cdot\boldsymbol{\nabla} \tag{A.5}$$

Along the stationary bottom Γ_B and the other fixed boundary Γ_{r2}, a no-flow condition is prescribed as,

$$\overline{\frac{\partial\phi}{\partial n}} = 0 \qquad \text{on } \Gamma_B \text{ and } \Gamma_{r2} \tag{A.6}$$

The time updating is performed by integrating the fully nonlinear free-surface boundary conditions A.3 and A.4 using a Lagrangian Taylor series expansions of the free surface position $\mathbf{r}$ and potential ϕ.

Appendix B. Convergence of the model results as a function of the discretization

Here, a convergence analysis is presented for two solitary waves of incident height $H_0' = 0.6$ shoaling over different plane slopes (see Figure 1). The configuration $S100\_H60$, with s = 1:100, leads to spilling wave breaking, while $S015\_H60$, with s = 1:15, leads to plunging wave breaking. These two configurations have different spatial resolutions since their domain lengths L' also differ (see Table 1). The sensitivity of the breaking onset parameters is evaluated for a variety of spatial resolutions in order to verify that the simulations are both accurate in terms of mass and energy conservation and have adequately converged.

The reference discretization of the BEM grid is the highest resolution case, which has $N = 1038$ nodes distributed along the free surface ($N_f = 838$ nodes) and the bottom, left, and right boundaries of the computational domain. Here, different spatial resolutions are tested, defined as a percentage of nodes with respect to the reference discretization (which thus has 100% of the nodes).

Table B.1: Convergence of the position of wave breaking onset x_c as a function of the computational domain discretization for the $S100\_H60$ configuration.

Simulations	N_f	nd. per λ	x_c at t_b
100% of nodes	838	212	44.47
90% of nodes	755	191	44.46
80% of nodes	671	170	44.47
70% of nodes	587	149	44.40
60% of nodes	503	127	44.39
50% of nodes	419	106	44.39
40% of nodes	335	85	44.21
30% of nodes	251	64	43.95
20% of nodes	167	42	41.72

Table B.2: Convergence of the position of wave breaking onset x_c as a function of the computational domain discretization for the $S015\_H60$ configuration.

Simulations	N_f	nd. per λ	x_c at t_b
100% of nodes	838	376	40.24
90% of nodes	755	339	40.24
80% of nodes	671	301	40.25
70% of nodes	587	263	40.24
60% of nodes	503	226	40.23
50% of nodes	419	188	40.21
40% of nodes	335	150	40.17
30% of nodes	251	116	39.91
20% of nodes	167	77	37.69

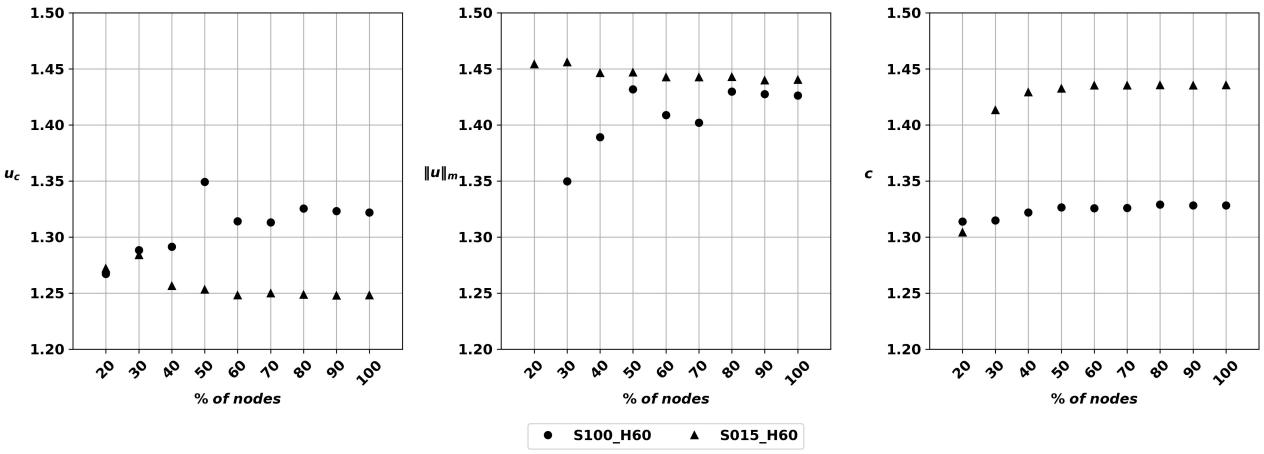

Figure B.1: Convergence analysis of the flow velocities u_c (left) and $\|\mathbf{u}\|_m$ (center) and of the wave phase velocity c (right) at t_b as a function of the BEM grid discretization for the two beach slope configurations.

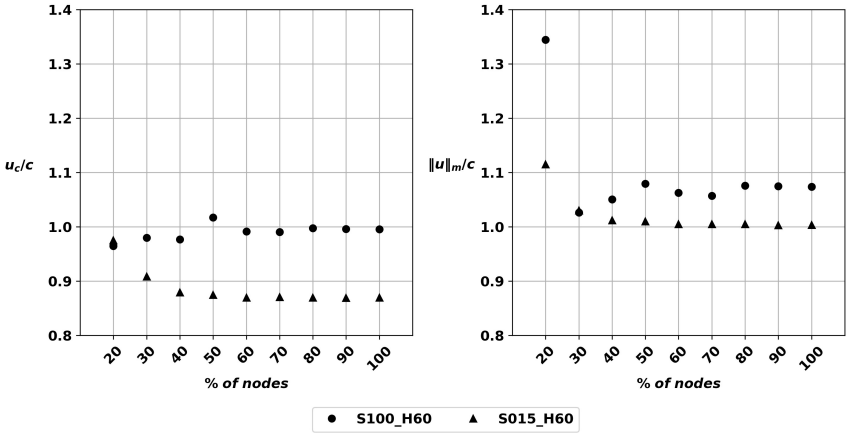

Figure B.2: Convergence analysis of the breaking onset criteria u_c/c (left) and $\|\mathbf{u}\|_m/c$ (right) at t_b as a function of the BEM grid discretization for the two beach slope configurations.

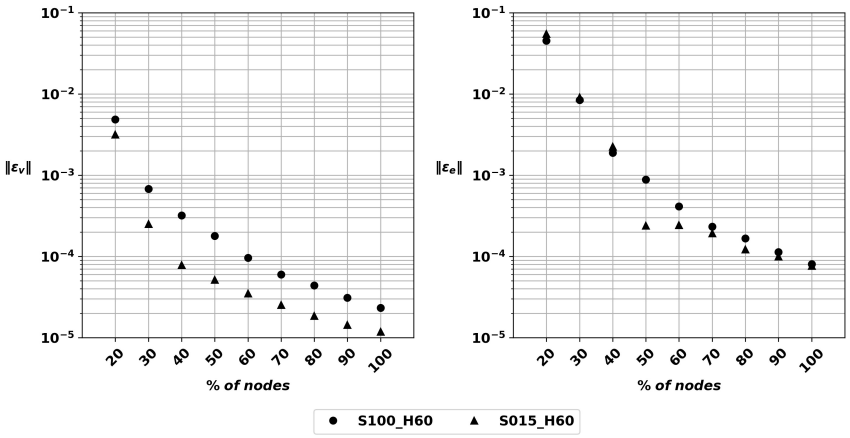

Figure B.3: Convergence analysis of the the maximum errors of mass ($\|\varepsilon_v\|$, left) and energy ($\|\varepsilon_e\|$, right) of the solitary wave at t_b as a function of the BEM grid discretization for the two beach slope configurations.

Figures B.1 to B.3 and Tables B.1 and B.2 show the simulation results for both beach slope configurations and all of the grid discretizations for the flow velocities u_c and $\|\mathbf{u}\|_m$, the wave phase velocity c, the breaking onset criteria u_c/c and $\|\mathbf{u}\|_m/c$, and the maximum relative errors (in absolute value) of the wave volume and energy, $\|\varepsilon_v\|$ and $\|\varepsilon_e\|$, with respect to the initial values computed with the method of [47].

For the $S015\_H60$ configuration, the reference 100% node discretization has a very fine resolution, so the parameters in Figures B.1 and B.2 start converging for simulation with only a 60% node discretization. In contrast, the parameters for the $S100\_H60$ configuration only start converging for the simulation with a 80% node discretization. Importantly, Figure B.3 shows that both relative numerical errors on mass and energy of the incident wave decrease significantly to acceptable levels for the converged simulations (to less than or about 0.01%).

For the two configurations tested here, the convergence analysis results show that the reference discretization provides both converged and accurate results at t_b. This discretization is the basis for all the simulations

considered in this paper.

References

[1] I. A. Svendsen, Wave heights and set-up in a surf zone, Coastal Eng. 8 (1984) 303–329.

[2] M. S. Longuet-Higgins, R. W. Stewart, Radiation stress in water waves, a physical discussion with applications, Deep Sea Research 11 (1964) 529–563.

[3] M. S. Longuet-Higgins, Longshore currents generated by obliquely incident sea waves, 1, J. Geophys. Res. 75 (1970) 6778–6789.

[4] J. H. MacMahan, E. B. Thornton, A. J. Reniers, Rip current review, Coastal Eng. 53 (2006) 191–208.

[5] J. Battjes, H. Bakkenes, T. Janssen, A. Van Dongeren, Shoaling of subharmonic gravity waves, Journal of Geophysical Research: Oceans 109 (C2) (2004).

[6] G. Symonds, D. A. Huntley, A. J. Bowen, Two-dimensional surf beat: Long wave generation by a time-varying breakpoint, Journal of Geophysical Research: Oceans 87 (C1) (1982) 492–498.

[7] M. Derakhti, J. T. Kirby, Breaking-onset, energy and momentum flux in unsteady focused wave packets, Journal of Fluid Mechanics 790 (2016) 553–581.

[8] M. Derakhti, M. L. Banner, J. T. Kirby, Predicting the breaking strength of gravity water waves in deep and intermediate depth, Journal of Fluid Mechanics 848 (2018) R2.

[9] V. Roeber, Boussinesq-type model for nearshore wave processes in fringing reef environment, Ph.D. thesis, Honolulu, University of Hawaii at Manoa (2010).

[10] A. B. Kennedy, Q. Chen, J. T. Kirby, R. A. Dalrymple, Boussinesq modeling of wave transformation, breaking, and runup. i: 1d, Journal of waterway, port, coastal, and ocean engineering 126 (1) (2000) 39–47.

[11] F. Shi, J. T. Kirby, J. C. Harris, J. D. Geiman, S. T. Grilli, A high-order adaptive time-stepping TVD solver for Boussinesq modeling of breaking waves and coastal inundation, Ocean Modelling 43 (2012) 36–51.

[12] Z. Tian, M. Perlin, W. Choi, Energy dissipation in two-dimensional unsteady plunging breakers and an eddy viscosity model, Journal of Fluid Mechanics 655 (2010) 217–257.

[13] M. Kazolea, A. I. Delis, C. E. Synolakis, Numerical treatment of wave breaking on unstructured finite volume approximations for extended boussinesq-type equations, Journal of Computational Physics 271 (2014) 281–305.

[14] A. Miche, Mouvements ondulatoires de la mer en profondeur croissante ou décroissante. forme limite de la houle lors de son déferlement. application aux digues maritimes. Troisième partie. Forme et propriétés des houles limites lors du déferlement. Croissance des vitesses vers la rive, Annales des Ponts et Chaussées Tome 114 (1944) 369–406.

[15] J. A. Battjes, J. P. F. M. Janssen, Energy loss and set-up due to breaking of random waves, in: Proceedings of the 16th international conference on coastal engineering, ASCE, 1978, pp. 569–587.

[16] E. B. Thornton, R. T. Guza, Transformation of wave height distribution, J. Geophys. Res. 88 (C10) (1983) 5925–5938.

[17] J.-F. Filipot, F. Ardhuin, A unified spectral parameterization for wave breaking: From the deep ocean to the surf zone, Journal of Geophysical Research: Oceans (1978–2012) 117 (C11) (2012).

[18] S. Guignard, S. T. Grilli, et al., Modeling of wave shoaling in a 2D-NWT using a spilling breaker model, in: The Eleventh International Offshore and Polar Engineering Conference (ISOPE01, Stavanger, Norway, June 2001), Vol. 3, 116-123, International Society of Offshore and Polar Engineers, 2001.

[19] M. Tissier, P. Bonneton, F. Marche, F. Chazel, D. Lannes, A new approach to handle wave breaking in fully non-linear boussinesq models, Coastal Engineering 67 (2012) 54–66.

[20] S. T. Grilli, J. Horrillo, S. Guignard, Fully nonlinear potential flow simulations of wave shoaling over slopes: Spilling breaker model and integral wave properties, Water Waves (2019) 1–35.

[21] H. A. Schäffer, P. A. Madsen, R. Deigaard, A boussinesq model for waves breaking in shallow water, Coastal Engineering 20 (3-4) (1993) 185–202.

[22] P. A. Madsen, O. Sørensen, H. Schäffer, Surf zone dynamics simulated by a boussinesq type model. part i. model description and cross-shore motion of regular waves, Coastal Engineering 32 (4) (1997) 255–287.

[23] O. R. Sørensen, P. A. Madsen, H. A. Schaffer, Nearshore wave dynamics simulated by boussinesq type models, in: Coastal Engineering 1998, 1998, pp. 272–285.

[24] R. Cienfuegos, E. Barthélemy, P. Bonneton, Wave-breaking model for boussinesq-type equations including roller effects in the mass conservation equation, Journal of waterway, port, coastal, and ocean engineering 136 (1) (2010) 10–26.

[25] P. Stansell, C. MacFarlane, Experimental investigation of wave breaking criteria based on wave phase speeds, J. Phys. Oceanogr. 32 (2002) 1269–1283.
URL http://ams.allenpress.com/archive/1520-0485/32/5/pdf/i1520-0485-32-5-1269.pdf

[26] R. Kurnia, E. Van Groesen, High order hamiltonian water wave models with wave-breaking mechanism, Coastal engineering 93 (2014) 55–70.

[27] G. Wei, J. T. Kirby, S. T. Grilli, R. Subramanya, et al., A fully nonlinear boussinesq model for surface waves. part 1. highly nonlinear unsteady waves, Journal of Fluid Mechanics 294 (7) (1995) 71–92.

[28] C. H. Wu, H. M. Nepf, Breaking criteria and energy losses for three-dimensional wave breaking, J. Geophys. Res. 107 (C10) (2002) 3177, doi:10.1029/2001JC001077.

[29] M. L. Banner, W. L. Peirson, Wave breaking onset and strength for two-dimensional deep-water wave groups, Journal of Fluid Mechanics 585 (2007) 93–115.

[30] U. Itay, D. Liberzon, Lagrangian kinematic criterion for the breaking of shoaling waves, Journal of Physical Oceanography 47 (4) (2017) 827–833.

[31] J.-B. Song, M. L. Banner, On determining the onset and strength of breaking for deep water waves. Part I: Unforced irrotational wave groups, J. Phys. Oceanogr. 32 (2002) 2541–2558.
URL http://ams.allenpress.com/archive/2541-2558/32/9/pdf/i1520-0485-32-9-2541.pdf

[32] Z. Tian, M. Perlin, W. Choi, Evaluation of a deep-water wave breaking criterion, Physics of Fluids 20 (6) (2008) 066604.

[33] X. Barthelemy, M. Banner, W. Peirson, F. Fedele, M. Allis, F. Dias, On a unified breaking onset threshold for gravity waves in deep and intermediate depth water, Journal of Fluid Mechanics 841 (2018) 463–488.

[34] S. Grilli, M. Derakhti, J. Kirby, M. Banner, A unified formulation for predicting the breaking onset of gravity water waves from deep to shallow water: validation cases using a fully nonlinear potential flow model, in: Fall Meeting Abstract, AGU, 2018, pp. OS31D–1799.

[35] M. Derakhti, J. T. Kirby, M. L. Banner, S. T. Grilli, J. Thomson, A unified breaking onset criterion for surface gravity water waves in arbitrary depth, Journal of Geophysical Research (submitted) - arXiv:1911.06896 (preprint) (2020).

[36] S. T. Grilli, R. Subramanya, Numerical modeling of wave breaking induced by fixed or moving boundaries, Computational Mechanics 17 (6) (1996) 374–391.

[37] M. Perlin, J. He, L. P. Bernal, An experimental study of deep water plunging breakers, Physics of fluids 8 (9) (1996) 2365–2374.

[38] H. Qiao, J. H. Duncan, Gentle spilling breakers: crest flow-field evolution, Journal of Fluid Mechanics 439 (2001) 57–85.

[39] S. T. Grilli, J. Skourup, I. A. Svendsen, An efficient boundary element method for nonlinear water waves, Engineering Analysis with Boundary Elements 6 (2) (1989) 97–107.

[40] M. S. Longuet-Higgins, E. D. Cokelet, The deformation of steep surface waves on water. Part I. a numerical method of computation, Proc. Roy. Soc. Lond. A 350 (1976) 1–26.

[41] S. Grilli, R. Subramanya, I. Svendsen, J. Veeramony, Shoaling of solitary waves on plane beaches, Journal of Waterway, Port, Coastal, and Ocean Engineering 120 (6) (1994) 609–628.

[42] S. T. Grilli, M. A. Losada, F. Martin, Characteristics of solitary wave breaking induced by breakwaters, Journal of Waterway, Port, Coastal, and Ocean Engineering 120 (1) (1994) 74–92.

[43] S. Grilli, I. Svendsen, R. Subramanya, Breaking criterion and characteristics for solitary waves on slopes, J. of Waterway, Port Coast. Ocean Eng. 123 (3) (1997) 102–112.

[44] S. T. Grilli, J. Horrillo, Numerical generation and absorption of fully nonlinear periodic waves, Journal of Engineering Mechanics 123 (10) (1997) 1060–1069.

[45] S. T. Grilli, Depth inversion in shallow water based on nonlinear properties of shoaling periodic waves, Coastal Eng. 35 (1998) 185–209.

[46] D. H. Peregrine, Breaking waves on beaches, Annual Review of Fluid Mechanics 15 (1) (1983) 149–178.

[47] M. Tanaka, The stability of solitary waves, The Physics of fluids 29 (3) (1986) 650–655.

[48] S. Beji, J. A. Battjes, Numerical simulation of nonlinear wave propagation over a bar, Coastal Eng. 23 (1994) 1–16.

[49] A. Saket, W. L. Peirson, M. L. Banner, M. J. Allis, On the influence of wave breaking on the height limits of two-dimensional wave groups propagating in uniform intermediate depth water, Coastal Engineering 133 (2018) 159–165.

[50] B. R. Seiffert, G. Ducrozet, F. Bonnefoy, Simulation of breaking waves using the high-order spectral method with laboratory experiments: Wave-breaking onset, Ocean Modelling 119 (2017) 94–104.